Optical sectioning in optical resolution photo acoustic microscopy

Seongho Park, Jean-Claude Vial, Kwangseuk Kyhm

Research Article | Vol. 25, No. 16 | 7 Aug 2017 | OPTICS EXPRESS 18917
Optics EXPRESS

Optical sectioning in optical resolution photo acoustic microscopy

SEONGHO PARK,[1] JEAN-CLAUDE VIAL,[3,4] AND KWANGSEUK KYHM[1,2,*]

[1]*Department of Opto and Cogno-mechatronics, Pusan National University, Busan 46241, South Korea*
[2]*Department of Physics Education, Pusan National University, Busan 46241, South Korea*
[3]*Univ. Grenoble Alpes, LiPhy, F-38041 Grenoble Cedex 9, France*
[4]*jean-claude.vial@univ-grenoble-alpes.fr*
[*]*kskyhm@pusan.ac.kr*

Abstract: We report a novel optical resolution photoacoustic microscopy concept to obtain an axial resolution only by optical methods. The photoacoustic signal is generated through a non-radiative relaxation from a level that is populated by excited state absorption. This two-step excitation process of a single laser enables to achieve an optical sectioning without any acoustic selectivity, whereby a full optical resolution photoacoustic microscopy is obtained. We bring a proof of this concept using Rhodamine and Zinc Tetraphenylporphyrin dyes known for their efficient excited state absorption process.

OCIS codes: (110.0110) Imaging systems; (110.5120) Photoacoustic imaging.

References and links

1. R. A. Kruger, "Photoacoustic ultrasound," Med. Phys. **21**(1), 127–131 (1994).
2. A. Karabutov, N. B. Podymova, and V. S. Letokhov, "Time-resolved laser optoacoustic tomography of inhomogeneous media," Appl. Phys. B **63**(6), 545–563 (1996).
3. A. A. Oraevsky, S. L. Jacques, and F. K. Tittel, "Measurement of tissue optical properties by time-resolved detection of laser-induced transient stress," Appl. Opt. **36**(1), 402–415 (1997).
4. P. Beard, "Biomedical photoacoustic imaging," Interface focus, rsfs20110028 (2011).
5. L. V. Wang and S. Hu, "Photoacoustic tomography: in vivo imaging from organelles to organs," Science **335**(6075), 1458–1462 (2012).
6. V. Ntziachristos, "Going deeper than microscopy: the optical imaging frontier in biology," Nat. Methods **7**(8), 603–614 (2010).
7. S. Hu and L. V. Wang, "Neurovascular photoacoustic tomography," Front. Neuroenergetics **2**, 10 (2010).
8. S. Hu and L. V. Wang, "Optical-resolution photoacoustic microscopy: auscultation of biological systems at the cellular level," Biophys. J. **105**(4), 841–847 (2013).
9. E. M. Strohm, M. J. Moore, and M. C. Kolios, "Single Cell Photoacoustic Microscopy: A Review," IEEE J. Sel. Top. Quantum Electron. **22**(3), 137–151 (2016).
10. J. G. White, W. B. Amos, and M. Fordham, "An evaluation of confocal versus conventional imaging of biological structures by fluorescence light microscopy," J. Cell Biol. **105**(1), 41–48 (1987).
11. W. Denk, J. H. Strickler, and W. W. Webb, "Two-photon laser scanning fluorescence microscopy," Science **248**(4951), 73–76 (1990).
12. S. Y. Lee, Y. H. Lai, K. C. Huang, Y. H. Cheng, T. F. Tseng, and C. K. Sun, "In vivo sub-femtoliter resolution photoacoustic microscopy with higher frame rates," Sci. Rep. **5**, 15421 (2015).
13. Y. Yamaoka, M. Nambu, and T. Takamatsu, "Fine depth resolution of two-photon absorption-induced photoacoustic microscopy using low-frequency bandpass filtering," Opt. Express **19**(14), 13365–13377 (2011).
14. P. Sathy, R. Philip, V. P. N. Nampoori, and C. P. G. Vallabhan, "Photoacoustic Observation of Excited Singlet-State Absorption in the Laser-Dye Rhodamine 6g," J. Phys. D Appl. Phys. **27**(10), 2019–2022 (1994).
15. K. Rurack, *Standardization and Quality Assurance in Fluorescence Measurements I,* 1st ed. (Springer, 2008).
16. P. C. Beaumont, D. G. Johnson, and B. J. Parsons, "Laser flash photolysis studies of some rhodamine dyes - Characterisation of the lowest excited singlet state of Rhodamine 3B, Sulforhodamine B and Sulforhodamine 101," J. Chem. Soc., Faraday Trans. **94**(2), 195–199 (1998).
17. J. Wiedmann and A. Penzkofer, "Excited-State Absorption Cross-Sections in Rhodamine Dyes Determined after Molecular-Reorientation," Nuovo Cimento B **63**(1), 459–469 (1981).
18. A. Chehrghani and M. J. Torkamany, "Nonlinear optical properties of laser synthesized Pt nanoparticles: saturable and reverse saturable absorption," Laser Phys. **24**(1), 015901 (2014).
19. M. Frenette, M. Hatamimoslehabadi, S. Bellinger-Buckley, S. Laoui, S. Bag, O. Dantiste, J. Rochford, and C. Yelleswarapu, "Nonlinear optical properties of multipyrrole dyes," Chem. Phys. Lett. **608**, 303–307 (2014).
20. N. Srinivas, S. V. Rao, and D. N. Rao, "Saturable and reverse saturable absorption of rhodamine B in methanol and water," J. Opt. Soc. Am. B **20**(12), 2470–2479 (2003).

#295678 https://doi.org/10.1364/OE.25.018917
Journal © 2017 Received 12 May 2017; revised 19 Jul 2017; accepted 22 Jul 2017; published 27 Jul 2017
Corrected: 10 Aug 2017

Optics EXPRESS

21. J. M. Héritier, "Electrostrictive Limit and Focusing Effects in Pulsed Photo-Acoustic Detection," Opt. Commun. **44**(4), 267–272 (1983).
22. L. Wang, C. Zhang, and L. V. Wang, "Grueneisen Relaxation Photoacoustic Microscopy," Phys. Rev. Lett. **113**(17), 174301 (2014).
23. I. V. Larina, K. V. Larin, and R. O. Esenaliev, "Real-time optoacoustic monitoring of temperature in tissues," J. Phys. D Appl. Phys. **38**(15), 2633–2639 (2005).
24. T. Lee and J. Guo, "Highly Efficient Photoacoustic Conversion by Facilitated Heat Transfer in Ultrathin Metal Film Sandwiched by Polymer Layers," Adv. Opt. Mater. **5**(2), 1600421 (2017).
25. T. Buma, M. Spisar, and M. O'Donnell, "High-frequency ultrasound array element using thermoelastic expansion in an elastomeric film," Appl. Phys. Lett. **79**(4), 548–550 (2001).
26. C. Zhang, K. Maslov, and L. V. Wang, "Subwavelength-resolution label-free photoacoustic microscopy of optical absorption in vivo," Opt. Lett. **35**(19), 3195–3197 (2010).

1. Introduction

Photoacoustic imaging of solid or liquid samples (particularly for biological tissues) is an emerging imaging modality, where light excitation is coupled to acoustic detection via the photoacoustic effect. As acoustic emission is induced by light absorption via thermo-elastic expansion, optical absorption yields images through the photoacoustic effect. It was first used in the field of absorption spectroscopy, and has been introduced for biomedical applications in the mid-90s [1–3]. In photoacoustic imaging, samples are illuminated by pulsed lights, and acoustic waves generated from the illuminated absorbing regions are detected by acoustic sensors. However, photoacoustic imaging is highly sensitive to optical absorption and occurs specifically in the illuminated spot as opposed to optical scattering. As the resolution of photoacoustic imaging depends on both optical and acoustic resolution, either the acoustic-resolution photoacoustic microscopy (AR-PAM) or the optical-resolution photoacoustic microscopy (OR-PAM) [4–6] can be implemented in photoacoustic imaging.

AR-PAM relies on the fact that, while light scattering, in particular in biological tissues, deteriorates the spatial resolution, ultrasound waves are weakly scattered but able to propagate in a straight manner. Therefore, the images of optical absorption can be reconstructed with the ultrasound resolution. For practical imaging, an array of detectors is used. For example, 50 μm- and 20 μm-resolution in the lateral and axial directions can be achieved respectively at several mm depths of mouse brain tissues.

For the images of OR-PAM obtained by scanning a focused optical beam, the accessible depth range is limited due to scattering (<1 mm), but the lateral-resolution is relatively good with a few μm range in the optical diffraction limit. Because the photoacoustic technique is less sensitive than the fluorescence detection, strong pulsed excitation is necessary, which would cause power broadening effect. In this case, the lateral-resolution becomes ~4 μm [7]. As OR-PAM is a hybrid technique, the axial resolution of OR-PAM is not solely determined by optics. In a confocal configuration [8], the numerical aperture of the acoustic detector determines an axial resolution of ~20 μm for the ultrasound frequency in ~100 MHz range [7]. Improved resolutions have been reported [9] for the ultrasound in 1 GHz range, but the observation depth is limited to single cultured cells imaging. Although confocal configuration for the acoustic detection provides optical sectioning in the axial direction, it cannot be maintained while the laser is scanning. Hence, the fast scanning technique used in fluorescence confocal microscopy [10] is not suitable for this technique. Nonlinear fluorescence microscopy, such as non-resonant two photon excited fluorescence microscopy [11], can be considered since it is also able to give an efficient sectioning without any confocal detection but the generated excited state population is generally low for moderate excitation intensity.

Optics EXPRESS

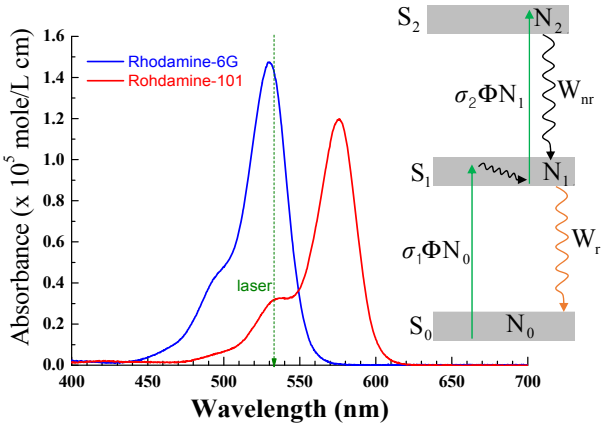

Fig. 1. Absorption spectra of Rhodamine-6G and Rhodamine-101 in methanol. The arrow indicates the wavelength of laser excitation. Schematics shows energy-level diagram of a Rhodamine molecule. Excitation of the ground state S_0 to the intermediate first excited state S_1 and excited state absorption from S_1 to the upper excited state S_2 are given by the corresponding population (N_0 and N_1), absorption cross section (σ_1 and σ_2), and laser fluence (Φ), respectively. While the transition from S_1 to S_0 is described by fluorescence with radiative decay rate (W_r), the transition from S_2 to S_1 is converted to acoustic vibration with non-radiative decay rate (W_{nr}).

In this work, we report a pure optical sectioning via optical nonlinearity for the optical resolution photoacoustic microscopy as a proof of concept, which is the so-called FOR-PAM (Full optical resolution photoacoustic microscopy). In the past few years, several groups have reported the two-photon excited acoustic contrast for microscopy [12,13], but the excitation in the infrared range causes a large one-photon background due to overtone absorption of the solvent [14]. In this case, a fancy filtering was necessary, and the setup became complicated. The FOR-PAM concept proposed in this work utilizes moderate excitation in the visible range and a filtering is not necessary because the involved optical nonlinear process is more efficient than other two-photon excitation effects.

2. Principle of FOR-PAM and theory

FOR-PAM utilises the ultrasound generated during the non-radiative relaxation in common organic dyes such as Rhodamine-6G and –101. As shown in Fig. 1, an optical transition from the ground state (S_0) to the intermediate first excited state (S_1) gives rise to a large absorption cross section, for example, near 532 nm in Rhodamine-6G. Since fluorescence from the first excited state (S_1) is known to have a quantum yield of near unity in methanol solvent [15], no sound is generated from the pure radiative transition from S_1 to S_0. However, S_1 can be excited to the upper excited state (S_2) with the same absorption wavelength for S_0-S_1 transition, which is known as excited state absorption (ESA) [16]. Relaxation from the S_2 state to S_1 is extremely fast (~100 fs) [17] and purely non-radiative. Consequently, FOR-PAM uses the sound produced by the non-radiative relaxation from S_2 to S_1, which is excited by ESA. Since two steps (S_0-S_1 and S_1-S_2 absorption) are needed to populate S_2, the sound intensity is expected to show a superlinear dependence on the excitation light intensity.

A slightly different mechanism will also be considered, it is associated to dyes characterised by a smaller cross section for the first excitation step but to compensate the weakness of the first step, the second step is highly efficient. In that case, ESA gives rise to a new phenomenon called RSA [18] (for Reverse Saturable Absorption) because, in opposition to classic ESA the laser absorption increases as the excitation power increases. A family of dyes has this behaviour: the multi-pyrrole dyes [19] among them the Zinc Tetra Phenyl Porphyrin (Zn:TPP) dye is particularly interesting because, despite a lower quantum

Optics EXPRESS

efficiency of the first excitation step, the second step is so efficient that the photoacoustic signal originates uniquely from the level attained by the second step.

In the following, the mathematical treatment of the dynamics is presented with parameters characteristics of the Rhodamine dyes, but the general features will be also valid for Zn:TPP.

Although several works reported the ESA and photoacoustic effect in Rhodamine dyes [14], required conditions for photoacoustic imaging have not been addressed. Therefore, we also analyse the experimental evidence of photoacoustic imaging with a theoretical model.

First of all, we confirm that the ESA is an efficient mechanism for populating the upper excited state S_2. Due to the wavelength proximity between the two photon absorption processes, a reverse saturation absorption (RSA) [20] can also be induced. The spectral positions of the excited and ground state absorption lines have been measured precisely [16]. Even if a small difference is present between the two spectral positions, the linewidth is broad enough to compensate it. In addition, we found that both the absorption cross sections of the first- (S_0-S_1) and the second-step (S_1-S_2) have the same order of magnitude. Sathy and associates [14] have already shown that ESA has a nearly quadratic dependence of the photoacoustic signal upon excitation fluence, but the reported fluence was very large compared to our results. Because a strong fluence likely gives rise to higher-order nonlinear effects, we use moderate excitation fluence.

In order to explain the photoacoustic signal generated by ESA, population dynamics in the three levels is considered [20] as shown schematically in Fig. 1. Rate equations of the populations (N_0, N_1, and N_2) at the level S_0, S_1, and S_2 can be given as:

$$N_0 + N_1 + N_2 = N, \tag{1}$$

$$\frac{dN_0}{dt} = -\sigma_1 \Phi \left(N_0 - N_1 \right) + W_r N_1, \tag{2}$$

$$\frac{dN_1}{dt} = \sigma_1 \Phi N_0 - \sigma_2 \Phi \left(N_1 - N_2 \right) - W_r N_1 + W_{nr} N_2, \tag{3}$$

$$\frac{dN_2}{dt} = \sigma_2 \Phi \left(N_1 - N_2 \right) - W_{nr} N_2, \tag{4}$$

where N is the total population. Regarding the transition between N_0 to N_1, optical absorption process from N_0 to N_1 gives rise to a decrease of the population change rate of N_0 (dN_0/dt), which involves the absorption cross section $\sigma_1 \sim 10^{-17}$ cm^2, the population difference between N_1 and N_0, and the laser fluence Φ of the 1 ns Gaussian pulse used. On the other hand, the radiative transition from N_1 results in an increase of dN_0/dt. The transition between N_1 to N_2 is governed by the ESA cross section $\sigma_2 \sim 10^{-17}$ cm^2 and the non-radiative transition. The vibrational relaxation within the intermediate levels of S_1 can be assumed to be instantaneous compared to the 1 ns laser pulse duration. In the case of Rhodamine, it is known [17] that the transition from N_1 to N_0 is mostly radiative with a rate of $W_r = 0.25$ ns^{-1} while the transition from N_2 to N_1 is dominated by the non-radiative decay rate $W_{nr} = 10$ ps^{-1}. Therefore, the fluorescence intensity from S_1 to S_0 and the photoacoustic signal intensity from S_2 to S_1 can be used as a measure of N_1 to N_2, respectively.

As shown in Fig. 2(a) and Fig. 2(b), the transient population N_1 and N_2 after a pulsed excitation are plotted for increasing Φ. For small Φ, N_1 increases linearly. However, it becomes saturated gradually for large $\Phi > 30$ mJ/cm^2. Such a typical saturation feature can be fitted by

$$N_1 \propto \frac{\Phi}{1 + \Phi / \Phi_{sat}}, \tag{5}$$

Optics EXPRESS

where the saturation fluence Φ_{sat} can be obtained as a fitting parameter. It is noticeable that a large fluence ($\Phi > \Phi_{sat} \sim 30$ mJ/cm^2) is necessary to saturate N_1. Unless an additional ESA transition from S_1 to S_2 is involved, N_1 would be saturated at a relatively small fluence.

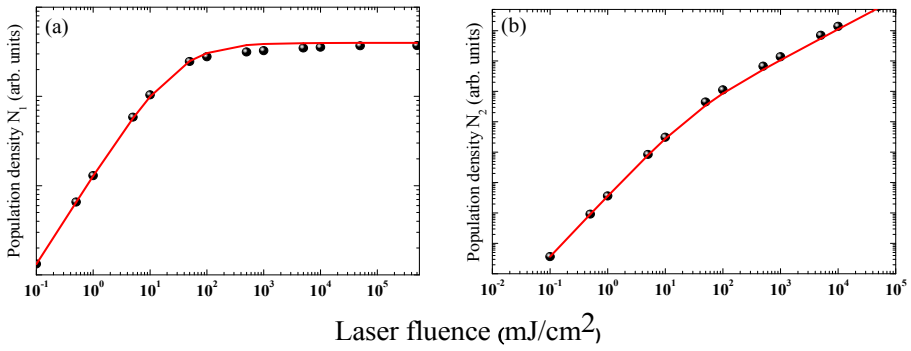

Fig. 2. Population density of the intermediate state (N_1) (a) and the upper excited state (N_2) (b) are obtained for increasing laser fluence, where the saturation of N_1 and N_2 are fitted by a first- and a second-order saturation model, respectively.

While N_2 is generated via N_1, the same wavelength of Φ for generating N_1 and N_2 is involved. Therefore, N_2 shows a quadratic dependence on Φ as shown in Fig. 2(b). Because the upper-level population becomes also saturated for large Φ, N_2 can be fitted by

$$N_2 \propto \frac{\Phi^2}{1+\Phi/\Phi_{sat}}, \tag{6}$$

where the same saturation fluence $\Phi_{sat} \sim 30$ mJ/cm^2 was obtained. From a practical point of view, the large saturation fluence ($\Phi_{sat} \sim 30$ mJ/cm^2) is advantageous because a high power laser excitation can be used without an excessive focus broadening. We performed experiments near the saturation range with a fluence of ~16 mJ/cm^2, which can be obtained by focusing a 50 nJ laser pulse down to a 10μm-radius spot.

3. Photoacoustic optical sectioning

For small fluence ($\Phi \ll \Phi_{sat}$), the quadratic dependence of the photoacoustic signal ($N_2 \sim \Phi^2$) can provide a sectioning image similar to that obtained in two-photon fluorescence microscopy. However, the power factor (α) of signal growth ($N_2 \sim \Phi^{\alpha}$) becomes less than 2 for large fluence ($\Phi > \Phi_{sat}$). Therefore, the sectioning becomes suppressed gradually as the quadratic signal growth becomes saturated.

Here we present a framework to predict this sectioning effect. When a Gaussian beam is focused along z-axis, the circular area perpendicular to z-axis $S(z) = \pi w_z^2$ is given as

$$S(z) = \lambda Z_R \left(1 + \frac{z^2}{Z_R^2}\right), \tag{7}$$

where the Rayleigh length $Z_R = \pi w_0^2/\lambda$ is determined by the minimum Gaussian beam waist w_0 at focus and the laser wavelength λ. Assuming the beam can be approximated as a top-hat intensity distribution, the fluence distribution is nearly uniform within the radius r(z). Because the sound signal $(z) is proportional to the total molecules within the uniform area S(z), $(z) can be obtained by integrating $N_2(x,y,z)$, as given in Eq. (6), over the *xy* plane of S(z) as

Optics EXPRESS

$$\$(z) = \int dxdyN_2(x,y,z) = N_2(z).S(z) \propto \frac{E^2}{S(z) + E/\Phi_{sat}}, \tag{8}$$

where E is the energy of a single laser pulse. Introducing Eq. (7) in Eq. (8) gives the following expression:

$$\$(z) \propto \frac{E^2}{\pi w_0^2\left(1+\Phi_0/\Phi_{sat}\right)} \quad \frac{1}{1+\dfrac{z^2}{Z_R^2\left(1+\Phi_0/\Phi_{sat}\right)}}, \tag{9}$$

where the beam spot size and fluence at focussing are respectively given by $\lambda Z_R = \pi w_0^2$ and

$$\frac{E}{\pi w_0^2} = \Phi_0.$$

Because Eq. (9) is a Lorentzian function of the distance from the focal point, z, the photoacoustic signal HWHM (half width at half maximum) corresponds to the excitation Rayleigh length for small fluence. As excitation fluence is increased, the width broadens as

$$HWHM = Z_R\sqrt{1+\frac{\Phi_0}{\Phi_{sat}}}. \tag{10}$$

Therefore, the sectioning effect is limited by the Rayleigh length and its broadening has a square root dependence for focused excitation fluence. Equation (9) is surely proportional to the initial acoustic pressure, but it depends on the technique used to measure the sound, the size, and the orientation of the laser point spread function. Additional terms for Eq. (8) have to be considered [21]. This point will be discussed later on.

4. Fluorescence depletion

Since the saturation occurs at the same fluence for S_1 (fluorescing level) and S_2 (non-radiative level), it is interesting to correlate the photoacoustic sectioning with the fluorescence signal as a function of laser focusing. With Eq. (5) and (7), an integration over a whole *xy* section gives the amount of fluorescing molecules as a function of the distance from focus z,

$$N_1S(z) \propto P\left(1-\frac{\dfrac{1}{1+\Phi_{sat}/\Phi_0}}{1+\dfrac{z^2}{Z_R^2(1+\Phi_0/\Phi_{sat})}}\right), \tag{11}$$

which has a Lorentzian-shaped dip (a fluorescence depletion) of width $HWHM = Z_R\sqrt{1+\dfrac{\Phi_0}{\Phi_{sat}}}$.

Optics EXPRESS

5. Experimental conditions

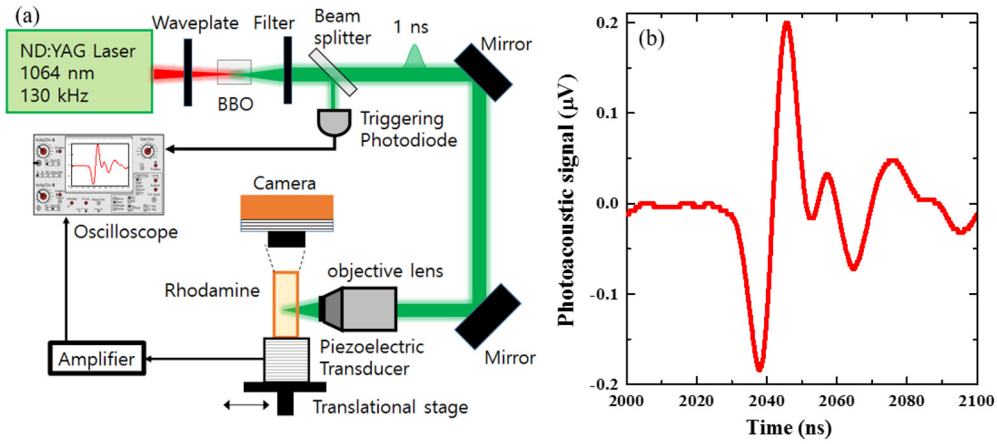

Fig. 3. (a) Schematics of experimental setup. (b) A typical photoacoustic signal generated from a Rhodamine 6G methanol solution under excitation of a 1ns-pulse laser with 532 nm wavelength.

The experimental setup is shown schematically in Fig. 3. Two different self Q-switched Nd:YAG lasers (SNP-130F-000 and SNP-20F- 100 of TEEM photonics) were used, which deliver the same 532 nm-wavelength radiation converted from the fundamental wavelength 1064 nm with a 1 ns pulse duration, but different pulse energy and repetition rate, 50 nJ at 130 KHz and 300 nJ at 20 KHz, respectively. The beam is collimated, expanded, and focused by a lens (focal distance = 75mm) for medium focusing or by a 10x objective lens (Mitutoyo, N.A = 0.28, focal distance = 20mm) to obtain a tighter focus. In that case, the focus parameters estimated from the beam radius at the objective pupil entrance are $w_0 = 1.1\mu m$ and $Z_R = 7\mu m$. These estimations are certainly optimistic because we are focusing inside a spectrometer cell (1.25mm of glass wall) while the objective is optimized for focusing in air, so that spherical aberrations are present. In addition the beam is not perfectly Gaussian ($M_2 = 1.5$) therefore the best focusing is, in fact, $w_0 = 1.5\mu m$.

To measure the photoacoustic sectioning, the acoustic signal, generated in a 100 μm thin cell, is measured as a function of the laser focus position by a high frequency (75 MHz), wide band pass piezoelectric transducer (Olympus, V2022) attached under the cell, and therefore the sample and the transducer are translated by a micrometric stage simultaneously. Two cascaded wideband amplifiers with 20 dB Gain (mini-circuit, ZFL-500 +) are used to amplify the signal which is accumulated 1000 times and averaged by a digital oscilloscope (LeCroy WaveSurfer 3000). For the fluorescence measurements, the thin cell is replaced by a wider one (1cm path). The fluorescence is collected perpendicularly to the exciting beam by a microscope objective and imaged by a CCD camera (Thorlabs, 1500M-GE-TE).

For the photoacoustic experiments, the concentration of Rhodamine dyes, dissolved in methanol, were adjusted so that about 50% of incident light at 532 nm was absorbed after propagating 100 μm. For the fluorescence measurements, the solutions are highly diluted to present an unnoticeable absorption though 1cm but to present a sufficient fluorescence intensity to be measured by the CCD camera.

For the photoacoustic sectioning measurement, depending on the resolution, the 100 μm size is penalizing so we will employ an alternative method inspired from the so called “Knife-Edge measurement” commonly used to measure the lateral size (the beam waist) of a laser. In our case, to measure the longitudinal photoacoustic response the equivalent of the knife is a wider (1 cm path) spectrometer cell filled with the dye and occupying a position above the acoustic transducer as shown on Fig. 3. The front surface of the dye exposed to the laser defines an abrupt interface between the inactive medium and the dye. The photoacoustic

Optics EXPRESS

signal is measured as a function of the laser focus position from this interface, the dye concentration being not too high to prevent an excessive attenuation of the laser at focus as it propagates into the cell. In that case the usual photoacoustic signal evolution as a function of the focus position is represented by a step function, the sectioning can then be obtained by the derivative of this step function.

6. Fluorescence

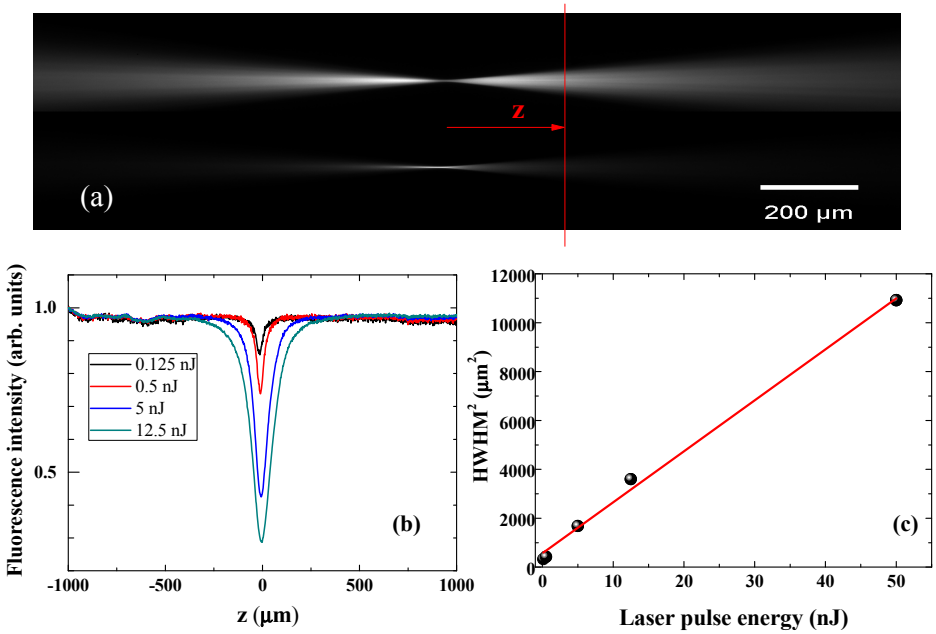

Fig. 4. (a) Fluorescence images in a highly diluted Rhodamine 101 solution under laser focusing, which is characterised in terms of beam waist (w_0 = 1.5µm) at focus and pseudo Rayleigh length Z'_R = 21 µm. Upper and lower images are of 50 nJ and 0.125 nJ laser excitation, respectively. (b) Integrated fluorescence intensity as a function of the distance from focus for various laser pulse energy. It is noticeable that the results are normalized by excitation pulse energy. (c) Square of the half width at half maximum (HWHM) for the signal dip in (b) is plotted for laser pulse energy, E, and fitted by $HWHM^2 = Z'^2_R(1 + E/E_{sat})$, whereby saturation energy, E_{sat}, can be obtained.

In order to characterise the tightly focused laser beam of 532 nm, we observe the fluorescence trace of a very dilute solution of Rhodamine 101. Figure 4 shows the two traces under 0.125 nJ and 50 nJ excitation, respectively. With strong 50 nJ excitation, a fluorescence diminution occurs at focus as a symptomatic saturation. A better way to characterise the focusing is to perform what we called an "integration profile" because we are collecting the fluorescence in the y-direction by a small numerical aperture microscope objective (NA<0.1), which has a large depth of focus, and the grey level distribution taken along a line (y-axis) perpendicular to z-axis is proportional to the sum of photons (proportional to the fluorescence power) emitted by a plane perpendicular to z. Therefore by performing an integration along the direction x for each z-coordinate, (using the plot profile function of ImageJ) we obtained the "integrated profile". Figure 4 shows the integrated fluorescence profile evolution as a function of the excitation pulse energy. As expected for an optical saturation, which is also in accordance with Eq. (11), we observe dips, which become broadened for increasing excitation power. Their widths (HWHM) evolution is also shown in Fig. 4, which can be described as $HWHM = Z'_R\sqrt{1+E/E_{sat}}$ whereby Eq. (6) can be verified with a "pseudo-Rayleigh length"

Optics EXPRESS

Z'_R = 21 µm. The data of Fig. 4 and a w_0 = 1.5 µm focusing also give Φ_{sat} = 32 mJ/cm^2. This saturation fluence is close to the value obtained in our numerical simulation.

Saturation alone is not interesting since it causes broadening for focusing, and also penalizes the radial and lateral resolution. Nevertheless, in the frame of the FOR-PAM model, saturation is necessary for an efficient ESA itself and mandatory for the generation of intense photoacoustic signals. Therefore, a compromise has to be found.

7. Photoacoustic

In order to demonstrate the ability of ESA for an optical sectioning, which can be detected by photoacoustic signals, a thin sample of Rhodamine solution is positioned along the focused laser axis as shown in Fig. 3.

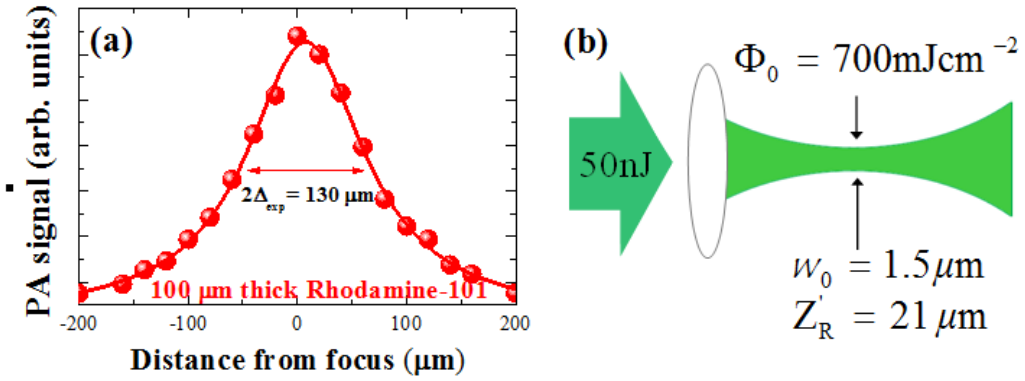

Fig. 5. (a) Photoacoustic signal generated in a 100 µm-thick film of Rhodamine-101 solution as a function of the distance (z). Dots are the experimental measurements and the solid curve is the best fit by a convolution of a Lorentzian (HWHM = 48µm) and a square function (100µm width) (b) Schematic drawing of experimental condition focus under 50 nJ excitation of 532nm laser, 1 ns pulse duration, w_0 = 1.5µm for maximum fluence of 700 mJ/cm^2, and length Z'_R = 21 µm.

Figure 5(a) shows a plot of the sound signal as a function of the position (z), which is generated from thin dye cuvette at various distances of the laser focus. Obviously, a sectioning effect is obtained as the sound signal strongly depends on the cuvette position. The half width at half maximum Δ_{exp} = 65 µm of this sectioning was observed to be approximately three times the pseudo-Rayleigh length. It is noticeable that not only the focusing conditions limit Δ_{exp}. Both a power broadening and the sample thickness of 100 µm can also affect the limit. In particular, the last contribution can be taken into account by considering that, in the first approximation, the experimental sectioning function is a convolution of the real sectioning function and the geometrical limits of a dye cuvette. While a Lorentzian function is assumed for the real sectioning function, a square function can be used for the 100 µm-thick dye cuvette. The convolution product of a Lorentzian and a square function is given by

$$\text{PA signal} \sim \tan^{-1}\left[\frac{(z+50)}{\Delta}\right] - \tan^{-1}\left[\frac{(z-50)}{\Delta}\right], \qquad (12)$$

where 50 µm is the half width of the dye cuvette, and Δ is the half width at half maximum of the Lorentzian real sectioning function. As shown in Fig. 5(a), the best fit with the experimental points was obtained with Δ = 48 µm. It is noticeable that the HWHM value (Δ = 48 µm) is 2.3 times the pseudo-Rayleigh length of the excitation beam. In our case, a high

Optics EXPRESS

fluence is necessary to give rise to a measurable signal. Therefore, the larger HWHM can be attributed to power broadening due to the high fluence.

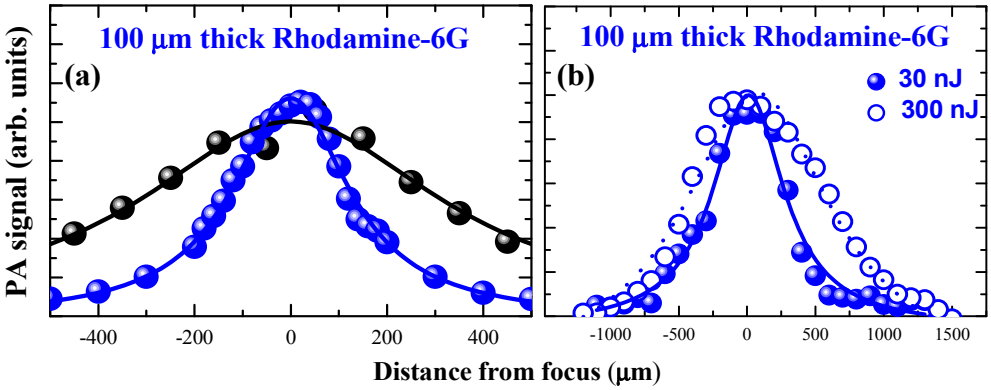

Fig. 6. (a) z-dependence of photoacoustic signal in a 100µm-thick film of Rhodamine-6G solution (blue) is compared to that in a thin metallic film (black) under 13 nJ excitation (532 nm, 1 ns pulse duration, w_0 = 2.5µm for maximum fluence of 66 mJ/cm^2, and length Z'_R = 60 µm). (b) Two z-dependence of normalized photoacoustic signals in a 100µm thick film of Rhodamine 6G solution under 300 nJ and 30 nJ laser excitations (532 nm, 1 ns pulse duration, w_0 = 6 µm and length Z'_R = 250 µm).

Figure 6(a) confirms that the sectioning capability of Rhodamine-101 is similar to that of Rhodamine-6G, which is known to show an efficient ESA [14], a very high quantum yield, and a particularly large absorption cross section at 532 nm (see Fig. 1). For this experiment, the beam was less tightly focused and the excitation power was reduced, in order to avoid damage on a thin metallic film used for comparison as explained later on. The sectioning effect obtained on the Rhodamine 6G is also noticeable. The sectioning value HWHM = 146 µm is about 2.4 times the pseudo-Rayleigh length.

Although the results of Rhodamine 6G and Rhodamine 101 look similar qualitatively, those cannot be strictly compared. At 532 nm, the absorption cross sections are different, and the saturation broadening is certainly different. Nevertheless, in both cases, the sectioning length is larger than the Rayleigh length. It is interesting to follow the sectioning capability as a function of excitation energy. For this test, the laser was focused by a lens with a relatively long focal length (75 mm). Figure 6(b) shows the photoacoustic sectioning for two laser energy values with the same dye (Rhodamine-6G). A broadening of the curve by a factor of 2 is observed as the energy is increased by a factor of 10. This confirms that a saturation starts to limit the sectioning even at the lowest fluence of 30 mJ/cm^2 at the focus.

One way to limit the power broadening is to find a chromophore with a lower absorption cross section for the first step S_0-S_1 but the consequence is to reduce the sound intensity except if, to compensate the weakness of the first step, the second step is highly efficient. Zinc Tetra Phenyl Porphyrin (Zn:TPP) presents the desired behaviour, named RSA, as shown on Fig. 7(a): the photoacoustic signal intensity follows a quadratic law as a function of the excitation energy in the range 0 to 100 nJ. Above, a saturation starts to occur, but our experimental condition for sectioning will not use this regime. Therefore the sectioning capability of Zn:TPP is expected to be better than that of Rhodamine dyes.

Optics EXPRESS

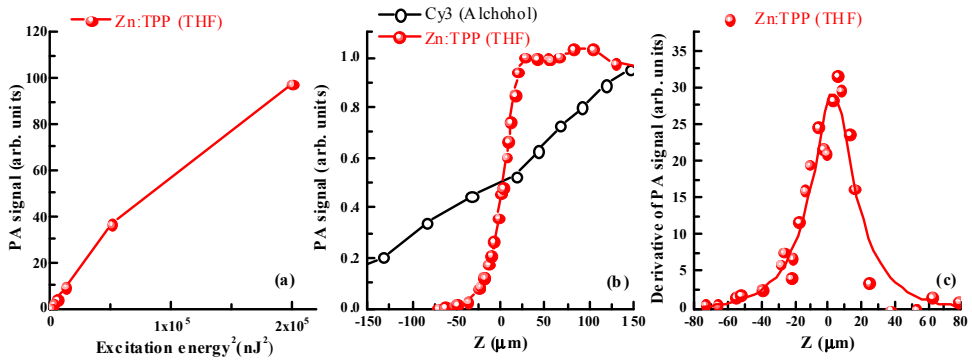

Fig. 7. (a) Photoacoustic signal intensity of a solution of Zn:TPP in THF (tetrahydrofuran) is plotted for the square of the laser excitation energy, where the laser is focused by a 0.28 NA objective. (b) Photoacoustic signal intensity as a function of the laser focus position (Z) from the entrance of a large cell filled with a THF solution of ZnTPP, or an alcoholic solution of Cy3, where the laser energy at 532 nm is 10 nJ and focused by a 0.28 NA objective. (c) Derivative of the Zn:TPP photoacoustic signal as a function of the focus position. The solid line is a Lorentzian fit with a HWHM = 15 µm.

In this experiment, since the Zn:TPP chromophore is a very efficient photoacoustic emitter, we were not limited by the laser power. This allowed us to overfill the entrance pupil of the objective, in order to obtain a narrower pseudo Rayleigh region (around 15 µm). The use of a 100 µm thick spectrophotometer cell is not ideal to evaluate the sectioning performance of this more efficient system, hence we employed the alternative method explained in the experimental section. Figure 7(b) shows the photoacoustic signal as a function of the distance from the laser focus to the entrance of the large cell. As expected a step shape is obtained and the same experiment done with a dye often use for photoacoustic imaging, Cyanine 3 (Cy3), shows a much less pronounced step.

The derivative of the above curve for Zn:TPP is straightforward, it represents the sectioning capability of this dye. It is shown on Fig. 7(c). Interestingly, with a HWHM = 15 µm the sectioning performance is much better than the sectioning obtained with the Rhodamine dyes, it approaches the Rayleigh length. It confirms that the broadening by saturation, present for the Rhodamine dyes, is the main limit of the method. To confirm the assertion that the predominant mechanism for FOR-PAM is the generation of ultrasound which follows the non-radiative relaxation of a level populated by ESA, we discuss hereafter other possible mechanisms for such a sectioning effect.

The temperature dependence of the Grueneisen parameter Γ is able to give a superlinear response since it increases with the temperature. Reference [22] gives an estimation of 3°C of temperature rise for an excitation fluence in the range of several J/cm^2. Our excitation fluence is far below this value. In addition, in the FOR-PAM concept, only one part of the excitation (the ESA) is transformed into heat. Therefore, in our experimental conditions, Γ is not expected to vary sufficiently [23] to bring a non-linear dependence of the photoacoustic signal upon the excitation fluence.

Our experimental arrangements, particularly the position of the piezoelectric sensor and the way to measure the signal (peak to peak values), are sensitive to the size of the laser beam as pointed out by Héritier [21]. Therefore, the sectioning can be a representative of the beam size variation along its focusing (a simple “size effect”). Our experimental conditions are not those used in [21]. To test this possibility, we performed experiments where only the size effect is present. Thin metallic films [24,25] are perfectly adapted for this test. Figure 6(a) shows that indeed a sectioning effect is present with a thin metallic film, but it is much less pronounced than the sectioning obtained with the Rhodamine dye excited in the same

Optics EXPRESS

conditions. We can assume that the sectioning function obtained with the Rhodamine represents the product of the pure optical sectioning function by the "size effect" function determined by the experiment on the metal film. Hence the pure optical sectioning function can be numerically obtained by performing the ratio of the Rhodamine experimental curve by the thin metal film curve. The result indicates that the "size effect" has a negligible effect as it induces only a 3% enhancement of the HWHM due to pure optical sectioning.

Another way to prove that the simple "size effect" can be neglected is shown on Fig. 7(b): the standard dye Cy3 dye, which is expected to have a linear (eventually sub linear) photoacoustic generation as a function of the laser fluence, is inefficient for sectioning compared to the Zn:TPP dye. Our experimental results are all in favour of an optical sectioning that originates from a non-linear (precisely superlinear) dependence of the photoacoustic signal upon the excitation fluence. For practical use, the irradiation conditions for FOR-PAM need to be in a range compatible with biomedical applications. Light fluences of several 100 mJ/cm^2 are common and even values up to 1000 mJ/cm^2 have been employed for in-vivo microscopy [26]. Therefore, our present conditions are acceptable.

Our results suggest that the first reason for sectioning degradation is the limited focusing. Combining spherical aberration correction and higher numerical aperture is expected to solve this issue to a great extent. Nevertheless, power broadening by saturation will be a limitation for dyes presenting a simple ESA. The mechanism of RSA [18] has to be preferred. In this case the quadratic dependence of the photoacoustic signal intensity as a function of the laser fluence provides a sectioning performance identical to that of the popular two-photon fluorescence microscopy technique. We can suggest that a two-laser setup can also be used to promote the efficiency of the ESA to a level comparable to RSA, opening the way to a larger variety of chromophores.

8. Conclusion

We use a photoacoustic mechanism in which sound is generated from a non-radiative relaxation of a level populated by a resonant two step absorption (ESA and RSA). It achieves an optical sectioning with an undetectable background. This concept enables enhanced axial resolution without the assistance of acoustic selectivity. Because conventional microchip laser has enough pumping power to generate the ESA and RSA for achieve this kind of mechanism, the acoustic microscopy setup can be simplified instead of heavy femto-laser systems. This is an advantage for practical application. It paves the way for a Full Optical-Resolution Photoacoustic Microscopy (FOR-PAM), and presents advantages analogous to that of two-photon excited fluorescence microscopy versus confocal microscopy. Under moderate laser fluence, we have measured an optical sectioning exceeding two to three times the Rayleigh length for simple ESA system while an efficient RSA system presents sectioning capabilities in the range of the Rayleigh length. We demonstrate that the main limitation is due to power broadening, which occurs when the optical transitions reach saturation, suggesting that axial resolution can be improved by increasing the detection sensitivity for ESA or favouring RSA systems. The performance of the technique can be further optimized by a judicious choice of excitation wavelength.

Funding

French program "AAP inter-instituts de la Mission pour l'Interdisciplinarité" (SuperPAM grant 2016); Korean Grant (NRF-2013M3C1A3065522, Pioneer research program).

Acknowledgment

We would like to thank Irene Wang for the careful reading of the manuscript and for the pertinent corrections she suggests. Prof. Mathieu Frenette and Prof. Jonathan Rochford are acknowledged for their help in the choice of the Zn:TPP.